Spin-energy entanglement of a time-focused neutron

Leiner, J.C.; Kuhn, S.J.; McKay, S.; Jochum, J.K.; Li, F.; Irfan, A.A.M.; Funama, F.; Mettus, D.; Parnell, S.R.; More Authors

DOI
10.1103/PhysRevApplied.22.L031005

Publication date
2024

Document Version
Final published version

Published in
Physical Review Applied

Letter

Spin-energy entanglement of a time-focused neutron

J.C. Leiner,[1,2,3,*,†] S.J. Kuhn,[1,†] S. McKay,[4,5,†] J.K. Jochum,[3] F. Li,[1] A.A.M. Irfan,[4,6] F. Funama,[1] D. Mettus,[2,3] L. Beddrich,[3] C. Franz,[7] J. Shen,[8] S.R. Parnell,[9] R.M. Dalgliesh,[10] M. Loyd,[1] N. Geerits,[11] G. Ortiz,[4,12,13] C. Pfleiderer,[2,3,14,15] and R. Pynn[4,5,12,16]

[1] *Neutron Technologies Division, Oak Ridge National Laboratory, Oak Ridge, Tennessee 37830, USA*
[2] *Physik-Department, Technische Universität München, Garching D-85748, Germany*
[3] *Heinz Maier-Leibnitz Zentrum (MLZ), Technische Universität München, Garching D-85748, Germany*
[4] *Department of Physics, Indiana University, Bloomington, Indiana 47405, USA*
[5] *Center for Exploration of Energy and Matter, Indiana University, Bloomington, Indiana 47408, USA*
[6] *Institute for Quantum Computing, University of Waterloo, Waterloo, Ontario N2L 3G1, Canada*
[7] *Jülich Centre for Neutron Science JCNS, Forschungszentrum Jülich GmbH Outstation at MLZ FRM-II, Garching D-85747, Germany*
[8] *Laboratory for Neutron Scattering and Imaging, Paul Scherrer Institut, Villigen 5232, Switzerland*
[9] *Faculty of Applied Sciences, Delft University of Technology, Mekelweg 15, Delft 2629 JB, Netherlands*
[10] *ISIS, Rutherford Appleton Laboratory, Chilton, Oxfordshire OX11 0QX, United Kingdom*
[11] *Atominstitut, TU Wien, Stadionallee 2, Vienna 1020, Austria*
[12] *Quantum Science and Engineering Center, Indiana University, Bloomington, Indiana 47408, USA*
[13] *Institute for Advanced Study, Princeton, New Jersey 08540, USA*
[14] *Center for Quantum Engineering (ZQE), Technische Universität München, Garching D-85748, Germany*
[15] *Munich Center for Quantum Science and Technology (MCQST), Technische Universität München, Garching D-85748, Germany*
[16] *Neutron Sciences Directorate, Oak Ridge National Laboratory, Oak Ridge, Tennessee 37830, USA*

(Received 5 April 2024; revised 9 July 2024; accepted 26 August 2024; published 25 September 2024)

Intraparticle entanglement of individual particles such as neutrons could enable another class of scattering probes that are sensitive to entanglement in quantum systems and materials. In this work, we present experimental results demonstrating quantum contextuality as a result of entanglement between the spin and energy modes (i.e., degrees of freedom) of single neutrons in a beam using a pair of resonant radio-frequency neutron spin flippers in the modulated intensity with zero effort configuration. We verified the mode entanglement by measuring a Clauser-Horne-Shimony-Holt contextuality witness S defined in the spin and energy subsystems, observing a clear breach of the classical bound of $|S| \leq 2$, obtaining $S = 2.40 \pm 0.02$. These entangled beams could enable alternative approaches for directly probing dynamics and entanglement in quantum materials whose low-energy excitation scales match those of the incident entangled neutron.

DOI: 10.1103/PhysRevApplied.22.L031005

Introduction. The multitude of demonstrations of the physical limits of determinacy inherent to quantum superposition and its extension, quantum entanglement [1], all point directly to their fundamental utility [2,3]. Quantum contextuality implies that even for observables at the same location in space and time (i.e., within a single particle [4]) there are still no hidden variables that determine observations [5]. In other words, the specific values for the observables are "decided" at the moment of measurement. Bell's theorem clarifies the way to rigorously distinguish between the case where particles hold information about their internal states or if those states are actually determined only at the instant of wave-function collapse. With carefully constructed experiments and closed loopholes supporting the latter case, it is becoming clear that quantum entanglement is an indispensable common element underlying fundamental physics, and may even be involved in the threads of spacetime itself [6–9].

In general, there is an intense motivation to develop methods that probe entanglement in a more direct manner in order to provide independent evidence and facilitate

*Contact author: leinerjc@ornl.gov, jleiner@alumni.nd.edu
†These authors contributed equally to this work.

observation of entanglement in materials [10,11]. However, determining whether a system is entangled typically requires careful linking of theory and experiment. The methods investigated in this work are designed to be *model agnostic*, which may allow direct extraction of information about quantum entanglement obtained from neutron spectroscopy experiments without the need for extensive modeling and prior knowledge of the sample's dynamics. Instead of analyzing only the neutron spectrum scattered from a sample with conventionally prepared neutron beams, proof-of-concept efforts have shown how one can utilize neutron beams that are themselves prepared in an entangled state in order to probe entangled samples [12].

By performing calibrated polarization measurements using a neutron resonant spin-echo (NRSE) instrument [13], we can obtain sufficient information on the correlations between the spin and energy observables of a single neutron to demonstrate the violation of a contextual Bell-like inequality [14–16]. Such a distinguishing demonstration is referred to as the construction and measurement of an *entanglement witness*. The theory used to extract information about the entanglement of a system from witness measurements is already well established [17,18]. This type of measurement essentially amounts to entangling the different degrees of freedom of individual neutrons in a way that can be verified with established neutron scattering instrument techniques. For instance, the energy, spin, and path subsystems of an individual neutron can be entangled with each other using an NRSE instrument [14]. Quantum contextuality is demonstrated by preparing and then experimentally measuring a Clauser-Horne-Shimony-Holt (CHSH) entanglement witness with the spin and path subsystems of the neutron [19] or by preparing a Mermin witness with tripartite entanglement of spin, path, and energy [20].

In this work, we demonstrate the entanglement of the energy and spin distinguishable subsystems within a neutron as it is manipulated by a variant of NRSE spectroscopy called MIEZE (Modulated IntEnsity with Zero Effort). This entanglement is demonstrated by measuring a CHSH witness value of 2.40 ± 0.02. This result is above the classical limit of 2 and corresponds to the expected value of a maximally entangled result of $2\sqrt{2} \times C$ where $C = 85\%$ is the MIEZE contrast (see Methods). Such a measurement substantiates the viability and practicality of preparing an entangled neutron beam with a time-focusing condition in contrast to conventional NRSE. In other words, this work (in contrast to previous work) demonstrates that an established spectroscopy technique, with permanently installed incarnations such as the RESEDA beamline at FRM-II [21,22], is intrinsically configured to exploit neutron spin-energy entanglement. Since the MIEZE technique already requires spin-energy correlations to achieve neutron measurements of dynamical excitations with *both* high intensity and high resolution, it opens another potentially more effective and complementary avenue for intraparticle entanglement to serve as a probe for quantum materials, particularly in magnetic systems displaying a large degree of entanglement such as quantum spin liquids [23].

Methods. We first construct a particular CHSH witness using the spin (s) and energy (e) degrees of freedom of the neutron, which are treated as two distinguishable subsystems leading to the tensor-product Hilbert state space $\mathcal{H} = \mathcal{H}_s \otimes \mathcal{H}_e$ [15]. Both $\mathcal{H}_s$ and $\mathcal{H}_e$ describe two-level (i.e., qubit) subsystems: $\mathcal{H}_s$ is the usual subspace of a nonrelativistic two-component spin-1/2 spinor and $\mathcal{H}_e$ is the subspace spanned by two energy states. The energy subspace can be described as two dimensional because the neutron can only access two energy states at each specific instance in time. We denote the relative phases of the spin and energy states by α and γ, respectively. We now define two pairs of observables $\sigma^s(\alpha_i)$ and $\sigma^e(\gamma_i)$ with $i \in \{1,2\}$, which act on the corresponding subsystems; these operators are associated with azimuthal angle α_i (γ_i) in the x-y plane of the corresponding Bloch spheres:

$$\sigma^s(\alpha_i) = \cos\alpha_i\,\sigma_x^s + \sin\alpha_i\,\sigma_y^s, \tag{1a}$$

$$\sigma^e(\gamma_i) = \cos\gamma_i\,\sigma_x^e + \sin\gamma_i\,\sigma_y^e. \tag{1b}$$

The projectors $P^s(\alpha_i)$ and $P^e(\gamma_i)$ for the observables $\sigma^s(\alpha_i)$ and $\sigma^e(\gamma_i)$ are defined, respectively, as

$$P^s(\alpha_i) = |\alpha_i\rangle\langle\alpha_i|, \quad |\alpha_i\rangle = \frac{|\uparrow\rangle + e^{i\alpha_i}|\downarrow\rangle}{\sqrt{2}}, \tag{2a}$$

$$P^e(\gamma_i) = |\gamma_i\rangle\langle\gamma_i|, \quad |\gamma_i\rangle = \frac{|E_+\rangle + e^{i\gamma_i}|E_-\rangle}{\sqrt{2}}. \tag{2b}$$

Next, we define the CHSH witness S as

$$S = E(\alpha_1,\gamma_1) + E(\alpha_1,\gamma_2) + E(\alpha_2,\gamma_1) - E(\alpha_2,\gamma_2), \tag{3}$$

where the joint expectation values $E(\alpha_i,\gamma_j)$ for $i,j \in \{1,2\}$ are defined as

$$E(\alpha_i,\gamma_j) = \langle\psi|\sigma^s(\alpha_i)\sigma^e(\gamma_j)|\psi\rangle \tag{4}$$

for a state $|\psi\rangle \in \mathcal{H}$. By decomposing each observable into two projectors (geometrically represented by the antipodal points on the equator of the Bloch sphere), we can write each expectation value as

$$E(\alpha_i,\gamma_j) = \frac{\sum_{k,l}(-1)^{k+l}N(\alpha_i + k\pi, \gamma_j + l\pi)}{\sum_{k,l}N(\alpha_i + k\pi, \gamma_j + l\pi)}, \tag{5}$$

with $k,l \in \{0,1\}$. It follows that to determine each expectation value, measurements of at least four different phase-shift settings are needed, namely $\{N(\alpha_i + k\pi, \gamma_j + l\pi)\}$ with $k,l \in \{0,1\}$.

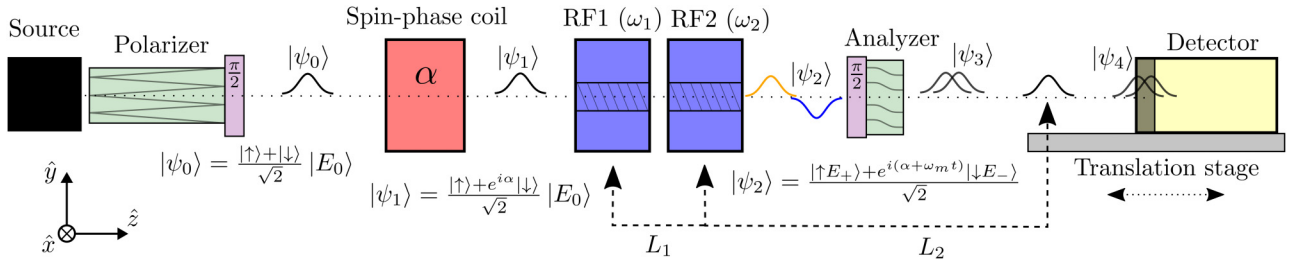

FIG. 1. Evolution of the total neutron wave function through the MIEZE instrument. After emerging from the polarizing V cavity and first $\pi/2$ flipper, the spin-phase coil tunes the spin phase of the neutron state $|\psi_0\rangle$ according to Eq. (8), resulting in the state $|\psi_1\rangle$. After the spin-phase coil, the neutron wave function is split both energetically and spatially by the first rf flipper (RF1), resulting in a maximally entangled Bell state [26]. After the second rf flipper (RF2) and second $\pi/2$ flipper, the state is given by $|\psi_2\rangle$, which is still maximally entangled. The analyzer acts like a projective measurement in the spin subsystem, producing an intensity oscillation in time, which is then measured by the detector. The detector is mounted on a longitudinally translating stage that adjusts the relative energy phase γ given by Eq. (14). Additional weak magnetic guide fields in the $\hat{y}$ direction are not shown. The states $|\psi_3\rangle$ and $|\psi_4\rangle$ are both given by Eq. (12). The wavepacket sizes and spatial separations are greatly enhanced for clarity.

No classical assignments of eigenvalues of observables by a local hidden variable theory can violate the CHSH inequality $|S| \leqslant 2$, but quantum mechanical expectations can [24]. The maximum value for S set by quantum mechanics is the Tsirelson bound of $2\sqrt{2}$ [25]. Therefore, we have a straightforward criteria to detect the presence of quantum correlations, namely

$$|S| \leqslant 2 \quad \text{(classical statistics)},$$
$$|S| \leqslant 2\sqrt{2} \quad \text{(quantum statistics)}.$$

Any state violating the CHSH inequality is necessarily an entangled state in the spin and energy degrees of freedom. For the witness given in Eq. (3), the maximum violation of the CHSH inequality occurs when $\alpha_1 + \gamma_1 = -\pi/4$ and $\alpha_2 - \alpha_1 = \gamma_2 - \gamma_1 = \pi/2$ [15].

We now present a detailed description of the neutron state manipulations performed by a prototypical MIEZE beamline as shown in Fig. 1, thereby connecting the experimental measurement to the evaluation of the witness. The standard MIEZE setup consists of two resonant rf neutron spin flippers operated at different frequencies to create an intensity modulation of the neutron wave function after polarization analysis, resulting in a time-oscillating signal [27,28]. In the absence of additional magnetic fields, this beating frequency, commonly called the *MIEZE frequency*, is given by

$$\omega_m = 2(\omega_2 - \omega_1), \tag{6}$$

where ω_1 (ω_2) is the angular frequency of the first (second) rf flipper. Quantum mechanical treatments of the NRSE and MIEZE techniques have previously been described [29,30], and their relevant aspects are included later in this section. Additional details on the derivation of the entanglement witness and the necessary approximations are provided within the Supplemental Material [31].

The experiment was performed on the CG-4B polarized test beamline at the High-Flux Isotope Reactor (HFIR) at Oak Ridge National Laboratory (ORNL), following initial measurements at FRM-II's RESEDA instrument [31]. At CG-4B, the neutron beam is prepared by a silicon monochromator with wavelength 0.55 nm and bandwidth $\Delta\lambda/\lambda \approx 0.2\%$ [32]. The neutrons are then polarized using a V cavity, ensuring that they have a well-defined initial spin state (96% average polarization). They then pass through a $\pi/2$ flipper that initiates the neutron precession, creating a superposition of spin-up and spin-down states:

$$|\psi_0\rangle = \frac{|\uparrow\rangle + |\downarrow\rangle}{\sqrt{2}}|E_0\rangle, \tag{7}$$

where E_0 is the initial neutron energy and the quantization axis is chosen to be in the guide field direction (the $\hat{y}$ direction in Fig. 1). After exiting the first $\pi/2$ flipper, the neutron travels through a static-field spin-phase coil, which produces a small magnetic field that is used to tune the neutron spin phase α. The relative spin phase is given by the usual Larmor precession formula:

$$\alpha = \frac{\gamma_n m \lambda}{h} \int d\ell\, \mathbf{B}(\ell), \tag{8}$$

where $\gamma_n > 0$ is the *magnitude* of the neutron gyromagnetic ratio, m the neutron mass, λ the neutron wavelength, and $\int d\ell\, \mathbf{B}(\ell)$ the magnetic field integral experienced by the neutron along the path ℓ through the coil. The field integral contribution from the spin phase coil is well approximated by $\int d\ell\, \mathbf{B}(\ell) \approx BL$ for a field region of length L and uniform field strength B. The input state to the first rf flipper up to a global phase factor is thus

$$|\psi_1\rangle = \frac{|\uparrow\rangle + e^{i\alpha}|\downarrow\rangle}{\sqrt{2}}|E_0\rangle. \tag{9}$$

The neutron then proceeds through the two rf flippers, which in the MIEZE configuration are run at different frequencies. The first rf flipper (RF1) running at a frequency ω_1 coherently changes the energy of the spin-up and spin-down states of the neutron. The change in energy corresponds to a change in velocity, and thus the up and down spin states separate spatially along the beamline ($\hat{z}$ in Fig. 1). The resonant spin flip in the first rf flipper entangles the incident polarized neutron in spin and energy [15,33]:

$$|\uparrow E_0\rangle \mapsto |\downarrow E'_-\rangle, \quad |\downarrow E_0\rangle \mapsto |\uparrow E'_+\rangle,$$

where $E'_\pm = E_0 \pm \hbar\omega_1$. Immediately after exiting the first rf flipper, the wave function of the neutron is then given up to a global phase factor by the maximally entangled Bell state [26]

$$|\psi_{\text{Bell}}\rangle = \frac{|\uparrow E'_+\rangle + e^{i(2\omega_1 t-\alpha)}|\downarrow E'_-\rangle}{\sqrt{2}}. \tag{10}$$

For more details on the origin of the relative phase in Eq. (10), see Refs. [34,35]. After exiting the second rf flipper (RF2), which again flips the neutron spin and changes the relative kinetic energy, the two states are longitudinally separated, with the lagging spin state having a greater energy; the neutron wave function up to a global phase factor is given by

$$|\psi_2\rangle = \frac{|\uparrow E_+\rangle + e^{i(\alpha+\omega_m t)}|\downarrow E_-\rangle}{\sqrt{2}}, \tag{11}$$

where $E_\pm = E_0 \pm \hbar(\omega_2 - \omega_1)$; this state is still a maximally entangled Bell state. After the final $\pi/2$ flipper and the spin analyzer, which transmits only the spin-up state, the resulting neutron state becomes

$$|\psi_3\rangle = \frac{1}{2}\left[|E_+\rangle + e^{i(\alpha+\omega_m t)}|E_-\rangle\right]|\uparrow\rangle. \tag{12}$$

Note that the neutron state after the analyzer is no longer mode entangled between the spin and energy subsystems as the analyzer acts as the projection operator $P^s(\alpha = 0)$ shown in Eq. (2a). Together, the spin-phase coil and analyzer act as a general projection operator $P^s(\alpha)$ for the spin subsystem.

In a typical MIEZE experiment, the detector is placed at the focusing point z_f where the two wave packets recombine such that $|\langle z_f|E_+\rangle|^2 = |\langle z_f|E_-\rangle|^2$. Complete recombination occurs only at a single point in space, but if the longitudinal beam coherence length $\beta_\ell = \lambda^2/\Delta\lambda$ is appreciably larger than the longitudinal spatial separation of the two spin states when the neutron is detected, then there is effectively a finite region of recombination [36–38]. The region of recombination is determined by the MIEZE focusing condition given by

$$\frac{L_1}{L_2} = \frac{\omega_2 - \omega_1}{\omega_1} + \frac{\gamma_n BL}{2\omega_1 L_2}, \tag{13}$$

where L_1 is the distance between the two rf flippers, L_2 the distance between the second rf flipper and the detector, and BL the field integral due to the spin-phase coil [39]. This equation is simplified to neglect the length of the rf flipper itself and the static fields between the rf flippers (see Ref. [40] for a more complete focusing equation). Notice that the focusing condition does not depend on the wavelength of the neutron, which is key to the effectiveness of the MIEZE technique since more neutrons from the source can be utilized. If allowed to further propagate, the wave packets begin to spatially separate once more, resulting in the defocused state $|\psi_4\rangle$ shown in Fig. 1, which is mathematically equivalent to Eq. (12). When the focusing condition is applied, the relative energy phase at the detector position takes the simple form

$$\gamma = -\frac{m\lambda\omega_m}{h}\delta, \tag{14}$$

where δ is the displacement of the detector from the focusing point. Therefore, at some point δ away from z_f for a particular detector time channel t_i, we measure the neutron intensity as

$$|\psi_\delta(t_i)|^2 = \frac{1 + \cos(\alpha + \gamma + \omega_m t_i)}{2}, \tag{15}$$

which is equivalent to an $N(\alpha, \gamma)$ term in Eq. (5), again up to a global phase factor and fit parameters. Taking $\gamma = 0$ at the focusing point, we must scan the detector longitudinally to adjust the energy phase (see Fig. 1). Therefore, the location of the detector and kinematic recombination of the two states act as a general projection operator $P^e(\gamma)$ for the energy subsystem. From this analysis, we have shown that the spin phase coil, rf flippers, second $\pi/2$ flipper, analyzer, and detector mathematically represent a joint projective measurement with projection operator $P^s(\alpha)P^e(\gamma)$, allowing us to measure the CHSH witness defined in Eq. (3).

Results. The beamline was prepared in the MIEZE configuration using transverse rf flippers with high-temperature superconducting (HTS) coils generating the static magnetic field with HTS films at the boundaries to ensure sharp field transitions and improve field homogeneity [41–43]. The frequency of the first rf flipper was set at $f_1 = 45$ kHz and the second at $f_2 = 50$ kHz, resulting in a MIEZE frequency $\omega_m/(2\pi) = 10$ kHz, which can be pushed into the MHz regime in the future [31,44,45]. The distance between the rf flippers was $L_1 = 85$ mm, which

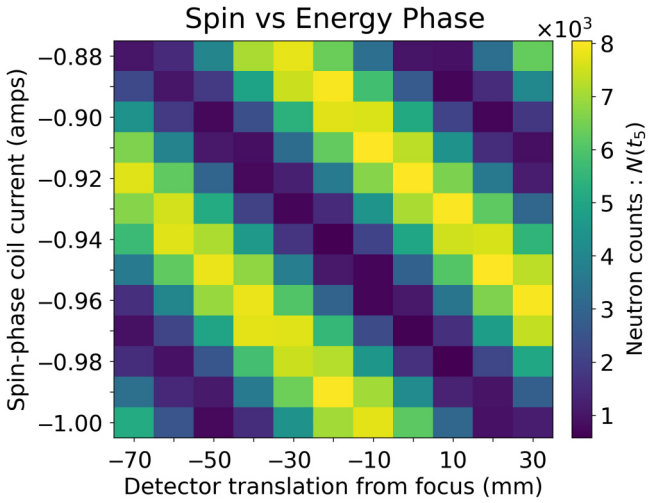

FIG. 2. Relative intensities (see Ref. [31] Sec. B for more details) collected at specific detector translation positions and scanned through the spin phase α at each detector position δ relative to the MIEZE focusing condition [see Eq. (13)], which is proportional to the energy phase γ [see Eq. (14)]. The frequencies of RF1 and RF2 were set at 45 and 50 kHz, respectively. Negative values represent translation away from the analyzer.

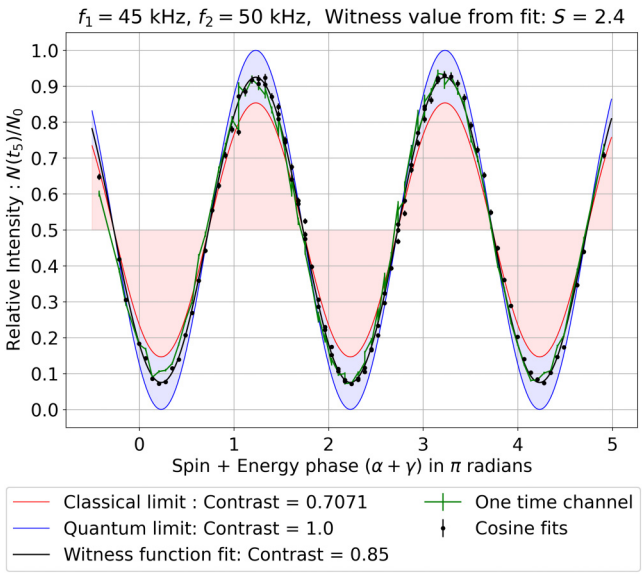

FIG. 3. Data from Fig. 2 fitted with $A + B\cos(\alpha + \gamma)$ in accordance with Eq. (15) and with the extracted parameters A and B, the commensurate witness value is then calculated from Eqs. (5) and (3). The blue colored area indicates the regime where the witness value S is strictly quantum, while the red area indicates values of S that can arise from quantum or classical correlations. The error bars are shown for the measured intensities, which indicate the standard deviations resulting from counting statistics.

with a balanced guide field integral along the beamline [$BL = 0$ in Eq. (13)] sets $L_2 = 765$ mm. The measurements consisted of independently scanning the spin and energy phases. The spin phase α is adjusted by tuning the current in the HTS spin phase coil, which consisted of two rectangular coils in Helmholtz configuration surrounded by HTS films. The field integral of the coil changes by $BL \approx 250$ m T mm per ampere of applied current. A 2π phase shift of α required a field integral of about 25 m T mm, corresponding to approximately a 0.1 A change in current (see Fig. 2). Therefore, the spin-phase current was scanned from -1.00 to -0.88 A in 0.01 A steps. The other guide fields through which the neutron passes together contribute a small constant value to the spin phase; this additional global phase was neglected as the guide fields were not changed during the experiment. Neutrons were counted with an Anger camera [46] mounted on a translation stage. A detector translation range of 70 mm covered a 2π energy-phase-shift range as shown in Fig. 2.

The normalized intensities [31] at the combined α and γ phases was fit with a global cosine function $A + B\cos(\alpha + \gamma)$ as shown in Fig. 3. The fitted parameters A and B were used to determine the expectation values defined by Eq. (5). These expectation values $E(\alpha, \gamma)$ were applied to the CHSH witness [Eq. (3)], which yielded a value of 2.40 ± 0.02, well above the classical limit of 2; the observed witness value is also the maximum possible value with our 85% MIEZE contrast, determined by the same fit.

Conclusion. Based on recent theoretical and experimental work regarding mode-entangled neutron beams [12,14–16], we have applied the theoretical procedure to rigorously construct a spin-energy entanglement witness using established MIEZE instrument configurations. The effectiveness of high energy-resolution neutron spin-echo spectroscopy techniques such as MIEZE fundamentally comes from labeling neutrons of varying energies with commensurate Larmor spin precessions. The procedure for witnessing spin-energy entanglement demonstrated here points to the utilization of the quantum properties of Larmor-labeled neutrons in inelastic neutron spectroscopy. High contrast and phase stability are the key requirements that must be ensured. The next steps will be to measure how suitable samples change the CHSH quantum contextuality witness value. Of note, with the MIEZE setup it is clear that the spin measurement at the analyzer is the point where the beam loses its spin-energy entanglement, and therefore the difference in signal with a sample placed before and after the analyzer would clarify the effects of an entangled neutron beam. Thus, this work represents a significant iteration toward a more direct and accessible method for probing entanglement in quantum materials.

Acknowledgments. The authors gratefully acknowledge Doug Kyle, Kaleb Burrage, Lowell Crow, Goran Nilsen, and Mark Davenport for their assistance with

experiments. Financial support by the German Bundesministerium für Bildung und Forschung (BMBF, Federal Ministry for Education and Research) through the Project No. 05K19W05 ("Resonante Longitudinale MIASANS Spin-Echo Spektroskopie an RESEDA") and Project No. 05K22WO2 ("Transportierbare Vorrichtung zur räumlichen Intensitätsmodulation (SIM-Mode) von polarisierten Neutronenstrahlen am FRM-II") is gratefully acknowledged.

We gratefully acknowledge financial support by the Deutsche Forschungsgemeinschaft (DFG, German Research Foundation) under TRR 360 (Project No. 492547816), the excellence cluster MCQST under Germany's Excellence Strategy EXC-2111 (Project No. 390814868), and the European Research Council (ERC) through Advanced Grant 788031 (ExQuiSid). This experiment was also attempted on the Larmor instrument at the ISIS Neutron and Muon source (UK) supported by a beamtime allocation RB2310511 from the Science and Technology Facilities Council [47].

This material is based upon work supported by the U.S. Department of Energy, Office of Science, Office of Workforce Development for Teachers and Scientists, Office of Science Graduate Student Research (SCGSR) program. The SCGSR program is administered by the Oak Ridge Institute for Science and Education for the DOE under Contract No. DE-SC0014664. This work was supported by the US Department of Energy (DOE), Office of Science, Office of Basic Energy Sciences, Early Career Research Program Award (KC0402010,ERKCSA4), under Contract No. DE-AC05-00OR22725. This research used resources at the High Flux Isotope Reactor, a DOE Office of Science User Facility operated by the Oak Ridge National Laboratory. G.O. gratefully acknowledges support from the Institute for Advanced Study. S.J.K. was partially supported by and the rf flipper used in Oak Ridge was constructed and optimized by Department of Energy STTR grants DE-SC0021482, DE-SC0018453 and DE-SC0023624.

[1] G. Aubrun *et al.*, Phys. Rev. Lett. **128**, 160402 (2022).
[2] A. Kitaev *et al.*, Phys. Rev. Lett. **96**, 110404 (2006).
[3] J. Handsteiner, *et al.*, Phys. Rev. Lett. **118**, 060401 (2017).
[4] S. Azzini *et al.*, Adv. Quantum Technol. **3**, 2000014 (2020).
[5] O. Gühne, E. *et al.*, Rev. Mod. Phys. **95**, 011003 (2023).
[6] M. Van Raamsdonk *et al.*, Gen. Relativ. Gravit. **42**, 2323 (2010).
[7] S. Singha Roy *et al.*, Phys. Rev. B **101**, 195134 (2020).
[8] J. G. Richens *et al.*, Phys. Rev. Lett. **119**, 080503 (2017).
[9] E. Moreva *et al.*, Phys. Rev. A **89**, 052122 (2014).
[10] P. Hauke *et al.*, Nat. Phys. **12**, 778 (2016).
[11] N. Laflorencie *et al.*, Phys. Rep. **646**, 1 (2016).
[12] A. A. M. Irfan *et al.*, New J. Phys. **23**, 083022 (2021).
[13] R. Golub *et al.*, Phys. Lett. A **123**, 43 (1987).
[14] J. Shen *et al.*, Nat. Commun. **11**, 930 (2020).
[15] S. Lu *et al.*, Phys. Rev. A **101**, 042318 (2020).
[16] S. J. Kuhn *et al.*, Phys. Rev. Res. **3**, 023227 (2021).
[17] A. Scheie *et al.*, Phys. Rev. B **103**, 224434 (2021).
[18] P. Laurell *et al.*, Phys. Rev. Lett. **127**, 037201 (2021).
[19] Y. Hasegawa *et al.*, Nature **425**, 45 (2003).
[20] Y. Hasegawa *et al.*, Phys. Rev. A **81**, 032121 (2010).
[21] C. Franz *et al.*, J. Phys. Soc. Jpn. **88**, 081002 (2019).
[22] C. Franz *et al.*, Nucl. Instrum. Methods Phys. Res. A: Accel. Spectrom. Detect. Assoc. Equip. **939**, 22 (2019).
[23] J. Khatua *et al.*, Phys. Rep. **1041**, 1 (2023).
[24] N. Gisin *et al.*, Phys. Lett. A **154**, 201 (1991).
[25] B. S. Cirel'son, Lett. Math. Phys. **4**, 93 (1980).
[26] M. A. Nielsen *et al.*, *Quantum Computation and Quantum Information* (Cambridge University Press, Cambridge; New York, 2000).
[27] W. Besenböck *et al.*, J. Neutron Res. **7**, 65 (1998).
[28] J. Felber *et al.*, Found. Phys. **29**, 16 (1999).
[29] N. Arend *et al.*, Europhys. Lett. **96**, 42001 (2011).
[30] T. Keller *et al.*, in *Scattering* (Academic Press, London, 2002), Chap. 2.8.6, p. 1264.
[31] See Supplemental Material at http://link.aps.org/supplemental/10.1103/PhysRevApplied.22.L031005, which includes Refs. [16,21,34,35,39,45,46,48–55], for a derivation of the entanglement witness using wave packets and for more details on data collection and fitting.
[32] Note that with a standard MIEZE beamline, the bandwidth is much higher, for example $\Delta\lambda/\lambda \approx 12\%$ at the RESEDA beamline.
[33] S. Sponar *et al.*, Phys. Lett. A **374**, 431 (2010).
[34] R. Golub *et al.*, Am. J. Phys. **62**, 779 (1994).
[35] V. K. Ignatovich *et al.*, Am. J. Phys. **71**, 1013 (2003).
[36] J. Felber *et al.*, Phys. B: Condens. Matter **252**, 34 (1998).
[37] N. Arend *et al.*, Phys. Lett. A **327**, 21 (2004).
[38] A. G. Klein *et al.*, Phys. Rev. Lett. **50**, 563 (1983).
[39] J. K. Jochum *et al.*, Meas. Sci. Technol. **31**, 035902 (2020).
[40] N. Geerits *et al.*, Rev. Sci. Instrum. **90**, 125101 (2019).
[41] R. Dadisman *et al.*, Rev. Sci. Instrum. **91**, 015117 (2020).
[42] F. Li *et al.*, Nucl. Instrum. Methods Phys. Res. A: Accel. Spectrom. Detect. Assoc. Equip. **955**, 163300 (2020).
[43] S. J. Kuhn *et al.*, arXiv:2408.02438.
[44] J. Jochum *et al.*, Meas. Sci. Technol. **32**, 045902 (2021).
[45] J. C. Leiner *et al.*, in *EPJ Web of Conferences*, Vol. 272 (EDP Sciences, 2022), p. 02008.
[46] M. Loyd *et al.*, Nucl. Instrum. Methods Phys. Res. A: Accel. Spectrom. Detect. Assoc. Equip. **1058**, 168871 (2024).
[47] R. Pynn, *et al.*, RB2310511, STFC ISIS Facility (2023).
[48] R. B. Dingle, *Asymptotic Expansions: Their Derivation and Interpretation* (Academic Press, London, 1973).
[49] D. J. Tannor, *Introduction to Quantum Mechanics: a Time-Dependent Perspective* (University Science Books, Sausalito, Calif, 2007).
[50] W. Gerlach *et al.*, Z. Physik **9**, 349 (1922).
[51] J. E. Sherwood *et al.*, Phys. Rev. **96**, 1546 (1954).
[52] A. S. Losko *et al.*, Sci. Rep. **11**, 21360 (2021).
[53] F. Funama *et al.*, Rev. Sci. Instrum. **95**, 033304 (2024).
[54] C. J. Schmidt *et al.*, J. Phys. Conf. Ser. **251**, 012067 (2010).
[55] M. Köhli *et al.*, J. Phys. Conf. Ser. **746**, 012003 (2016).